

Ionization of the Xenon Fluorides

Christian Buth,* Robin Santra,† and Lorenz S. Cederbaum
*Theoretische Chemie, Physikalisch-Chemisches Institut, Ruprecht-Karls-Universität Heidelberg,
 Im Neuenheimer Feld 229, 69120 Heidelberg, Germany*
 (Dated: June 15, 2003)

The noble-gas atom xenon can bind fluorine atoms and form several stable compounds. We study the electronic structure of the xenon fluorides (XeF_n , $n = 2, 4, 6$) by calculating their ionization spectra using a Green's function method, which allows to treat many-body effects at a high level. Our focus is on the valence region and on the $\text{Xe}4d$ core hole. We observe a sensitive dependence of the spectra on the number of fluorine ligands. Systematic line shifts are uncovered and explained. In the $\text{Xe}5s$ and $\text{F}2s$ inner-valence regimes, from XeF_2 to XeF_6 , the usefulness of the one-particle picture of ionization is found to become progressively worse. Moreover, adding the electronegative fluorine ligands seems to enhance—not suppress—the Auger decay of a $\text{Xe}4d$ core hole.

I. INTRODUCTION

Noble-gas atoms are, in general, chemically rather inert. Nevertheless, since the heavy noble-gas species krypton, xenon, and radon possess a comparatively small ionization potential, they *can* form molecules, at least together with electronegative elements. The most stable and most widely investigated among these compounds are the xenon fluorides¹ XeF_2 , XeF_4 , and XeF_6 .

The electronic structure of the xenon fluorides has been the subject of a number of both experimental and theoretical investigations. In the 1970's, photoabsorption experiments, at photon energies between 50 and 160 eV^{2,3} and between 6 and 35 eV⁴, were carried out at DESY in Hamburg. Carroll *et al.*⁵ employed photoelectron spectroscopy to measure the chemical shifts of the $\text{F}1s$ and $\text{Xe}3d$ levels in the xenon fluorides. More recently, using synchrotron radiation, Cutler *et al.*⁶ obtained gas-phase photoelectron spectra with such a high resolution that fluorine-ligand field splittings on the $\text{Xe}4d$ levels could be extracted.

Photoelectron spectroscopy, in combination with *ab initio* studies, is an outstanding tool for characterizing the electronic structure of a molecule. However, at least in the case of the xenon fluorides, there exist—to our knowledge—only few theoretical contributions to motivate and back-up experimental work. The pioneering papers^{7–9}, which are more than 20 years old, utilized self-consistent-field methods to calculate ionization potentials. The restriction to an effective one-particle model made it impossible to uncover complexities due to electron correlation. Newer theoretical work^{10–12} on xenon fluorides focused on electronic ground-state geometries and dissociation energies. It is therefore timely to improve on the early studies and to explore some of the *many-body* physics of electrons in XeF_2 , XeF_4 , and XeF_6 . This is the purpose of this paper.

We proceed as follows. Section II describes the Green's function method we use to calculate ionization spectra. We discuss the molecular geometries we employed in our calculations, and we analyze the impact of relativistic effects on the ionization spectra of the xenon fluorides. The ionization spectra we calculated cover the valence

regime and the $\text{Xe}4d$ core line; they are presented in Sec. III. A detailed comparison between spectra that take electron correlation into account and spectra based on the Hartree-Fock model demonstrates the occurrence of many-body phenomena in almost the entire spectral regime we consider. These phenomena display an interesting dependence on the number of fluorine ligands. A summary and conclusions are given in Sec. IV.

II. COMPUTATIONAL DETAILS

A. Algebraic Diagrammatic Construction

Green's functions are a fundamental tool of many-body theory^{13–16}. They are well suited to calculating various properties of molecules^{17,18}. For instance, the pole positions of the one-particle propagator yield the vertical ionization potentials of a molecule. The residuum or pole strength of a pole of the one-particle propagator is a measure of the one-particle character of a specific ionized state, i.e. it is a measure how well the physical state is described within the one-hole configuration space deriving from the Hartree-Fock ground state.

Algebraic diagrammatic construction (ADC) is a sophisticated, systematic approximation scheme for Green's functions^{19–21}. The n -th order ADC scheme, $\text{ADC}(n)$ for short, contains infinite summations of those classes of Feynman diagrams that derive from the first n orders of the Feynman-Dyson perturbation series. The problem of finding the pole positions and pole strengths of a Green's function is formulated in terms of the solution of a Hermitian matrix eigenvalue problem.

The one-particle $\text{ADC}(3)$ scheme we use in this work to calculate ionization spectra employs the Dyson equation^{13,20}, which allows to sum many diagram classes in addition to the summation already carried out by the ADC scheme itself. Exploiting the validity of the Dyson equation necessitates the combined treatment of the ionization potentials *and* the electron affinities. The latter are also given by pole positions of the one-particle propagator. This approach enlarges the aforementioned ADC eigenvalue problem considerably. Therefore, the affinity

block in the ADC matrix is reduced in practice by performing on this block a few (typically ten) block Lanczos iterations²². The most important spectral features of the affinity block are preserved in this way, and the final eigenvalue problem to be solved becomes much more manageable.

The ionization potentials associated with the Xe 4d orbitals in the xenon fluorides lie far above the molecular double ionization threshold. Hence, not only two-hole-one-particle configurations but also three-hole-two-particle configurations are expected to have impact on the description of the core-level ionization spectra^{23–25}. The ADC(3) scheme does not contain three-hole-two-particle configurations explicitly, but the next-order scheme, ADC(4), does. Thus, one expects that the ADC(4) scheme yields an appreciable improvement of calculated core-level ionization spectra.

The inclusion of three-hole-two-particle configurations enlarges the configuration space—and the associated eigenvalue problem—extremely. The available computer resources would not be sufficient to calculate ionization spectra of molecules like XeF₆ in an acceptable amount of time. The existing ADC(4) programs^{24–26} therefore utilize the core-valence separation approximation²³ for core-level ionization, which reduces the size of the configuration space. This approximation, however, makes it impossible to calculate ionization potentials in the valence regime. Furthermore, since core-valence separation implies that all elements of the configuration space carry a core hole, those two-hole-one-particle configurations that are needed to describe core-hole decay are not included. For these reasons, the ADC(4) programs are useless for the questions we would like to address here. Hence, all ionization spectra were calculated within the ADC(3) scheme^{20,21}.

B. Geometries and Basis Sets

The ground-state geometries of F₂, XeF₂, XeF₄ and XeF₆ are taken from the literature. The distance of the fluorine atoms in the fluorine molecule is $r(F-F) = 1.42 \text{ \AA}^1$. Xenon(II)-fluoride is a linear molecule of $D_{\infty h}$ symmetry with a Xe–F distance of 1.977 \AA^1 . Xenon(IV)-fluoride is square-planar (D_{4h}), the Xe–F distance is 1.94 \AA . All distances given refer to molecules in the gas phase.

The ground-state geometry of xenon(VI)-fluoride in the gas phase is a distorted octahedron^{6,10}. It can be described in C_{3v} symmetry. Nevertheless, some of our computations on XeF₆ were performed in O_h symmetry to elucidate the impact of the reduced symmetry. The notation of Fig. 1a in Ref. 10 is used here. Our calculations on XeF₆ in C_{3v} symmetry use the bond lengths $r(\text{Xe-F1}) = 1.856 \text{ \AA}$ and $r(\text{Xe-F4}) = 1.972 \text{ \AA}$ and bond angles $\alpha = 80.8^\circ$ and $\beta = 112.8^\circ$. These values, which were determined using MP2 and an all-electron basis with f functions, were taken from Tables 2 and 3 in Ref. 10. Our

computations on XeF₆ in O_h symmetry were performed at the bond length $r(\text{Xe-F}) = 1.952 \text{ \AA}$, which is taken from Table 1 in Ref. 10.

The ADC programs^{22,26} (see Sec. II A) require molecular integrals and orbital energies. These were obtained in Hartree-Fock calculations using the GAMESS-UK²⁷ program package. The employed software does not exploit symmetry for the xenon atom. D_{2h} symmetry is used for F₂, XeF₂ and XeF₄. The calculation of the ionization potentials of XeF₆ in the ground-state geometry of C_{3v} symmetry is performed in C_s symmetry; for the geometry of O_h symmetry, GAMESS-UK assumes D_{2h} symmetry. Comparing the orbital energies from both the C_{3v} and the O_h geometry shows that the overall positions of the xenon-like orbitals are in good agreement in both symmetries, but the splitting of the fluorine-like orbitals is enlarged due to the increased interaction in C_{3v} symmetry²⁸.

The xenon and the fluorine atoms are represented by the DZVP (DFT orbital)^{29,30} basis set. The quality of the basis set can be estimated from Table I by comparing the numerically exact Hartree-Fock orbital energies (see the ensuing Sec. II C) of xenon with those obtained using the DZVP (DFT orbital) basis set. The shift of the orbitals, due to the approximation introduced by the finite basis set, is $\Delta\varepsilon_{\text{BS}} := \varepsilon_{\text{HF, numeric}} - \varepsilon_{\text{HF, DZVP}}$. The shift is $\approx 0.13 \text{ eV}$ for the Xe 4d orbitals and even less for the valence orbitals because basis sets are usually optimized with respect to the latter orbitals. This shift is neglected in the following, for other sources of inaccuracies are more significant.

C. Relativistic Effects

There are three main relativistic effects one has to take into account when examining heavy atoms like xenon^{31,32}:

1. the relativistic radial contraction and energetic stabilization of the s and p shells,
2. the spin-orbit splitting,
3. the relativistic radial expansion and the energetic destabilization of the (outer) d and f shells.

Effects (1) and (3) are termed scalar relativistic effects¹⁰.

As the theory of Sec. II A for the calculation of ionization potentials is strictly non-relativistic, one has to take into account relativistic effects by a “rule of thumb”. This is done by performing for the xenon atom Hartree-Fock calculations with MCHF84³³ and Dirac-Fock calculations, the relativistic counterpart to Hartree-Fock^{31,32}, with GRASP92^{34,35}. Due to the spherical symmetry of atoms, the equations can be solved without fixed basis sets to arbitrary precision. This gives exact sets of relativistic and non-relativistic orbitals in the mean-field approximation.

In Table I, the orbital energies determined in this way are listed together with Hartree-Fock orbital energies obtained by a calculation employing the DZVP (DFT Orbital) basis set. By comparing the orbital energies of the two numerical solutions of the Hartree-Fock and Dirac-Fock equations, one can determine the size of relativistic effects and correct for them in non-relativistic computations of the ionization potentials of the xenon fluorides.

In order to carry out this comparison, one has to note that the total angular momentum j results from coupling the orbital angular momentum l with the electron spin: $j = l \pm \frac{1}{2}$. A Dirac-Fock calculation yields, for $l \geq 1$, two orbitals³¹, one for $j_+ = l + \frac{1}{2}$ and one for $j_- = l - \frac{1}{2}$. The j_- orbital has a lower orbital energy than the j_+ orbital.

The spin-orbit splitting between the j_+ orbital and the j_- orbital can be effectively removed by calculating a weighted mean

$$\bar{\varepsilon}_{\text{DF}} = \frac{(2j_+ + 1)\varepsilon_{\text{DF},+} + (2j_- + 1)\varepsilon_{\text{DF},-}}{2j_+ + 1 + 2j_- + 1} \quad (1)$$

of the two Dirac-Fock orbital energies³¹. This procedure facilitates comparison between the Dirac-Fock and the Hartree-Fock calculation. The scalar relativistic shift of the non-relativistic orbitals is $\Delta\varepsilon := \bar{\varepsilon}_{\text{DF}} - \varepsilon_{\text{HF}}$. The shifts are 3.077 eV for the Xe 4d, -1.789 eV for the Xe 5s and -0.00283 eV for the Xe 5p orbitals. The sign of the shift $\Delta\varepsilon$ is predicted by the rules (1) and (3) given above, because the energetic stabilization of s and p orbitals leads to a lowering of the Xe 5s and Xe 5p orbital energies and thus $\Delta\varepsilon < 0$. Similarly, $\Delta\varepsilon > 0$ holds for the shift of the Xe 4d orbital energies due to the energetic destabilization of the (outer) d orbitals.

Koopmans' theorem^{16,36} states that the ionization potentials of an atom or a molecule are approximately given by the negative of the orbital energies, $IP \approx -\varepsilon_{\text{HF}}$. As the relativistic shift $\Delta\varepsilon$ represents a relativistic correction to the Hartree-Fock orbital energies $\varepsilon_{\text{HF,corr}} = \varepsilon_{\text{HF}} + \Delta\varepsilon$, the ionization potentials are corrected as follows: $IP_{\text{corr}} = IP_{\text{HF}} - \Delta\varepsilon$.

The mentioned shifts of the orbital energies of the xenon atom are used to correct the Xe 4d orbital energies for the scalar relativistic effect by adding $-\Delta\varepsilon$ to the Xe 4d ionization potential of the non-relativistic calculations. This procedure is justified by the observation that the molecular Xe 4d orbitals are highly localized and are very similar to atomic Xe 4d orbitals. The Xe 4d ionization potentials, calculated with the ADC(3) scheme, take electron correlation into account. Therefore, contributions of many orbitals mix into the description of the Xe 4d ionized states. Since the Xe 4d ionized states are predominantly described by the Xe 4d orbitals, the relativistic correction is applicable in this case as well.

The spin-orbit splitting in the xenon atom amounts to 2.111 eV for the 4d orbitals and 1.436 eV for 5p orbitals (see Table I). The spin-orbit splitting in the xenon atom is probably only a good approximation⁶ for the Xe 4d orbitals in the xenon fluorides, because the Xe 5p orbitals

suffer from a significant modification by the molecular bond to the fluorine atoms. The experimental value for the spin-orbit splitting of the 4d orbitals in the xenon atom is 1.984 ± 0.014 eV⁶ (see Table IV). The theoretically and experimentally determined values are in satisfactory agreement. A good agreement is not expected because the Dirac-Fock equations are based on a mean-field approximation³¹. Spin-orbit splitting is not accounted for in the non-relativistic theory used throughout and is not considered any further in the ensuing sections.

III. RESULTS AND DISCUSSION

A. Mean-Field Model

Single ionization spectra of the xenon fluorides can be obtained in the Hartree-Fock approximation with the help of Koopmans' theorem^{16,36}. In this mean-field model, the correlation between the electrons is neglected, resulting in very simple spectra (see Fig. 1) that can provide hints for the interpretation of the more complex spectra that include electron correlation (see Fig. 2). The assignment of the lines in Fig. 1 to atomic orbitals of xenon or fluorine is not strict in the valence region, due to the molecular bond. In the deeper lying molecular orbitals, this assignment is well defined. Since spin-orbit coupling is neglected, artificial degeneracies are introduced in the spectra of Fig. 1. The effect of the ligand field caused by the fluorine atoms is of course included.

The effect of adding fluorine atoms to xenon is studied in Table II by Mulliken and Löwdin population analyses^{16,37}. Such population analyses may exhibit some basis set dependence¹⁶, but the consistency between the two sets of results indicates reliability. One sees immediately that charge is withdrawn from the xenon atom to the fluorine atoms: 1.1 electron charges in XeF_2 , 1.9 in XeF_4 , and 2.3 in XeF_6 . Due to the C_{3v} symmetry of the ground-state geometry of XeF_6 , there are two kinds of fluorine atoms, with different distances to the central xenon atom. These differences in nuclear separation are reflected in Table II by the fact that fluorine atoms which are further away from the xenon atom acquire less charge.

At first sight one might assume that the computed change in charge density involves only the valence electrons and has little effect on the inner molecular orbitals of the xenon fluorides. In the hydrogen atom, the wave functions of the higher lying shells, which are unoccupied in the ground state, have a considerable amplitude in the spatial regions of the lower lying shells of the same angular momentum³⁸. As this argument also holds in the case of the xenon fluorides, a reduction of valence electron density on the xenon atom leads to a less efficient screening of its nuclear charge and consequently to a lowering in energy of the energetically low lying molecular orbitals with a dominant contribution on the xenon atom.

Conversely, the increase of valence electron density on

HF orbital	ε_{HF} , DZVP	ε_{HF} , numeric	DF orbital	ε_{DF}	$\bar{\varepsilon}_{DF}$
4d	-2.78280	-2.77788	4d _{3/2} 4d _{5/2}	-2.71133 -2.63376	-2.66479
5s	-0.946253	-0.944414	5s	-1.01014	-1.01014
5p	-0.457894	-0.457290	5p _{1/2} 5p _{3/2}	-0.492572 -0.439805	-0.457394

TABLE I: Hartree-Fock (HF) and Dirac-Fock (DF) orbital energies of xenon. Hartree-Fock orbital energies are given for the DZVP (DFT orbital)^{29,30} basis set and for the numerically exact solution³³. The Dirac-Fock orbital energies also are numerically exact^{34,35}. $\bar{\varepsilon}_{DF}$ is calculated using Eq. (1). All data are given in Hartree.

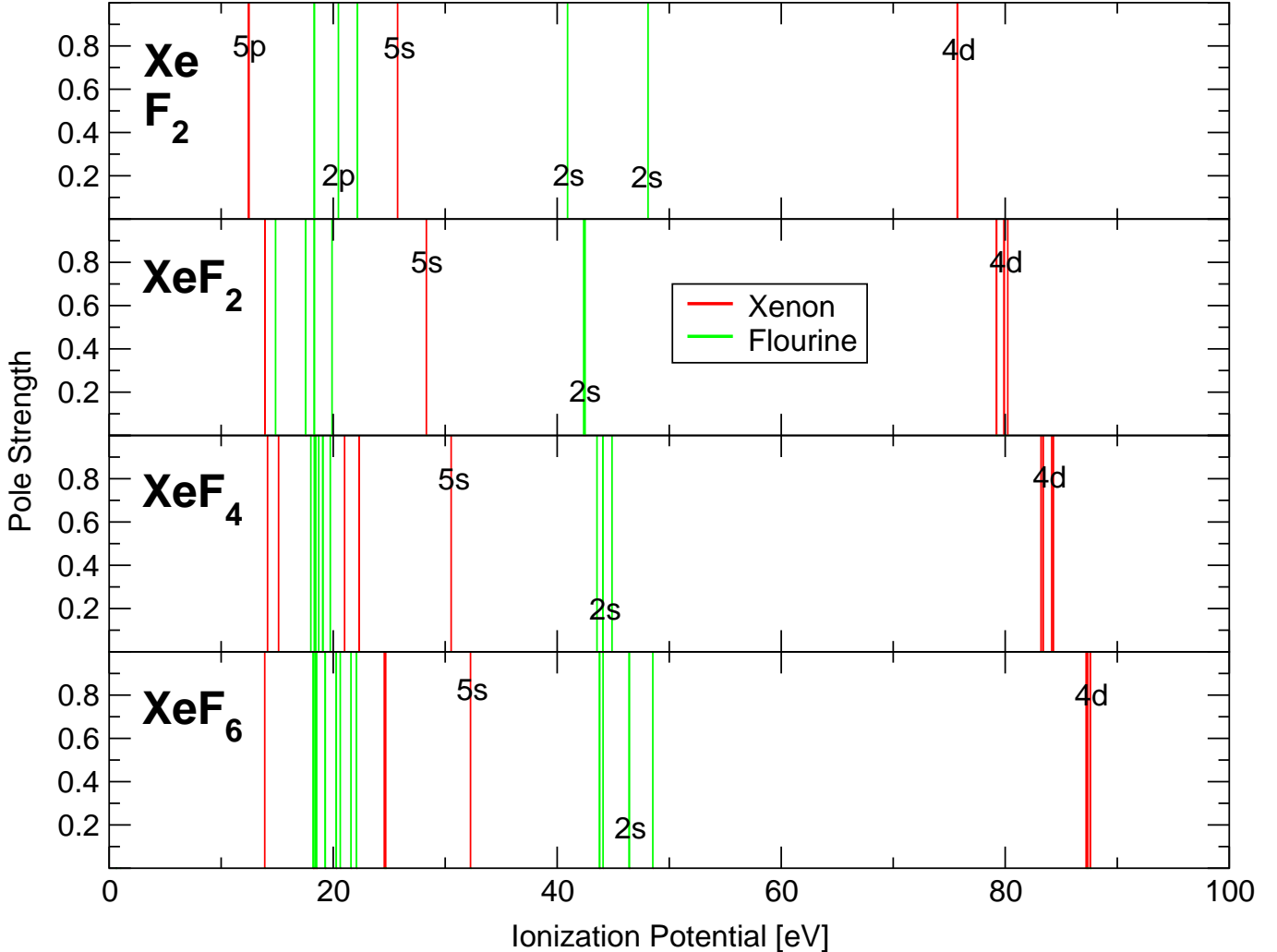


FIG. 1: (Color) Single ionization spectra of Xe, F₂, XeF₂, XeF₄, and XeF₆ calculated at the Hartree-Fock level (Koopmans' theorem). The assignment of the lines to atomic orbitals of xenon or fluorine origin in XeF_n is not strict in the valence region, due to the molecular bond.

the fluorine atoms leads to a more efficient screening of their nuclear charge and consequently raises the energy of the lower lying molecular orbitals with a dominant contribution on fluorine atoms. The charge withdrawn from the xenon atom is shared among several fluorine atoms. The net increase of charge density on each fluorine atom

is ≈ 0.5 electron charges. This value is, of course, much smaller than the loss of charge density on the xenon atom and hence the impact on the inner molecular orbitals of fluorine character is clearly much smaller than for xenon. It is most dramatic in XeF₂ where each fluorine atom acquires the largest fraction of charge. The screening of the

Compound	Atoms	Nuclear Charge	Mulliken Population	Löwdin Population
XeF_2	Xe	54	52.92	52.95
	2 F	9	9.54	9.53
XeF_4	Xe	54	52.13	52.12
	4 F	9	9.47	9.47
XeF_6	Xe	54	51.71	51.51
	3 F	9	9.49	9.51
	3 F	9	9.27	9.33

TABLE II: Mulliken and Löwdin population analyses of XeF_2 , XeF_4 , and XeF_6 .

nuclear charge is largest in XeF_2 and decreases in XeF_4 and XeF_6 .

The effects of this model can be seen in Fig. 1. The positions of the $\text{Xe } 5s$ and $\text{Xe } 4d$ lines shift to higher binding energies with an increasing number of fluorine atoms. The energy differences between the corresponding lines of XeF_2 and XeF_4 and of XeF_4 and XeF_6 are nearly equally large. The $\text{F } 2p$ and $\text{F } 2s$ lines also shift slightly to higher binding energies with increasing number of fluorine atoms. The charge redistribution over several fluorine ligands we mentioned earlier furnishes an explanation for the shift of the fluorine lines. This interpretation is further supported by a comparison with F_2 . The mean of the $\text{F } 2p$ lines in F_2 and the mean of the $\text{F } 2s$ lines in F_2 are higher in energy than the mean values of the corresponding lines in XeF_2 . The first ionization potential is nearly constant for all xenon fluorides studied. Its value is ≈ 12.5 eV.

In the fluorine molecule, the two $\text{F } 2s$ lines are split considerably due to the molecular bond. The splitting of the two $\text{F } 2s$ lines in XeF_2 is tiny due to the large separation of the fluorine atoms. In XeF_4 and XeF_6 , the fluorine atoms are closer and interact. This results in a larger splitting of the $\text{F } 2s$ lines in comparison to the splitting in XeF_2 .

The $\text{Xe } 4d$ lines are quintuply degenerate in the single ionization spectrum of the xenon atom in Fig. 1. In XeF_2 , the degeneracy is lifted by the ligand field of the fluorine atoms and three distinct lines become visible. The three lines reflect the spatial orientation of the $4d$ orbitals. There is a ligand field along the molecular axis. Perpendicular to the molecular axis there is no shift, resulting in a total of three lines. In XeF_4 there is only one dimension left that is unaffected by the ligand field: the axis perpendicular to the molecular plane. The spectrum, Fig. 1, shows that there are two distinct groups of $\text{Xe } 4d$ lines in this case.

In XeF_6 , the situation changes because the fluorine ligands are grouped around the xenon atom in such a way that XeF_6 is close to octahedral symmetry. O_h symmetry in XeF_6 leads to two distinct $\text{Xe } 4d$ orbital energies separated by only 0.1568 eV. Lowering the symmetry of XeF_6 to C_{3v} results in three distinct $\text{Xe } 4d$ orbital ener-

Compound	1 st Experimental IP	1 st ADC IP
Xe	12.129	12.16
XeF_2	12.35	12.76
XeF_4	13.1	13.07
XeF_6	12.35	12.56

TABLE III: Comparison of the calculated lowest (first) ionization potentials (IP) of Xe, XeF_2 , XeF_4 , and XeF_6 with experimental results. The first ionization potential of xenon is taken from Ref. 1. The other first ionization potentials are taken from Ref. 4. All data are given in electronvolt.

gies with a total splitting of 0.3682 eV, which is still small compared to the much larger $\text{Xe } 4d$ splittings in XeF_2 and XeF_4 .

B. Correlation Effects

Going beyond the Hartree-Fock description of the molecules by using ADC(3) leads to the ionization potentials plotted in Fig. 2. Figure 1 helps identify the one-particle origin of the states in Fig. 2. The $\text{Xe } 4d$ lines are energetically clearly separated from the outer and inner valence lines in all spectra. They are located between 72 eV and 82 eV. The $\text{F } 2s$ -derived lines are present between 35 eV and 45 eV. Correlation effects do not change the fact that the lowest ionization potentials are approximately equal in all compounds.

In fact, at the lowest ionization potentials, which are associated with the $\text{Xe } 5p$ levels, there is qualitative agreement between the correlated and the mean-field calculation: The pole strengths are very close to unity; the one-particle picture is valid. Nevertheless, ADC(3) improves on the Hartree-Fock method in a quantitative manner. In the correlated calculation, the energetically lowest cations are stabilized by about 1 eV relative to the respective one-particle energies. The first ionization potentials of xenon and its fluorides, as calculated within the ADC(3) scheme, are compared to the experimental results in Table III. The agreement of experimental and calculated ionization potentials is good.

At higher energies, there is typically not even qualitative agreement between mean-field and many-body treatment. Overall, there is a dramatic change of the ionization spectra due to the inclusion of many-body effects. The importance of electron correlation grows with increasing number of fluorine atoms. This is reflected in energy shifts and reduction of intensity in the outer valence part of the spectra; in the appearance of numerous satellite lines in the vicinity of 20 eV and above; and, in particular, in the eye-catching breakdown of the molecular orbital picture of ionization seen in the $\text{Xe } 5s$ and $\text{F } 2s$ inner-valence region.

The latter phenomenon is common in molecules³⁹: The intensity originally confined to a single orbital in Fig. 1 is spread over many cationic states (see Fig. 2). The

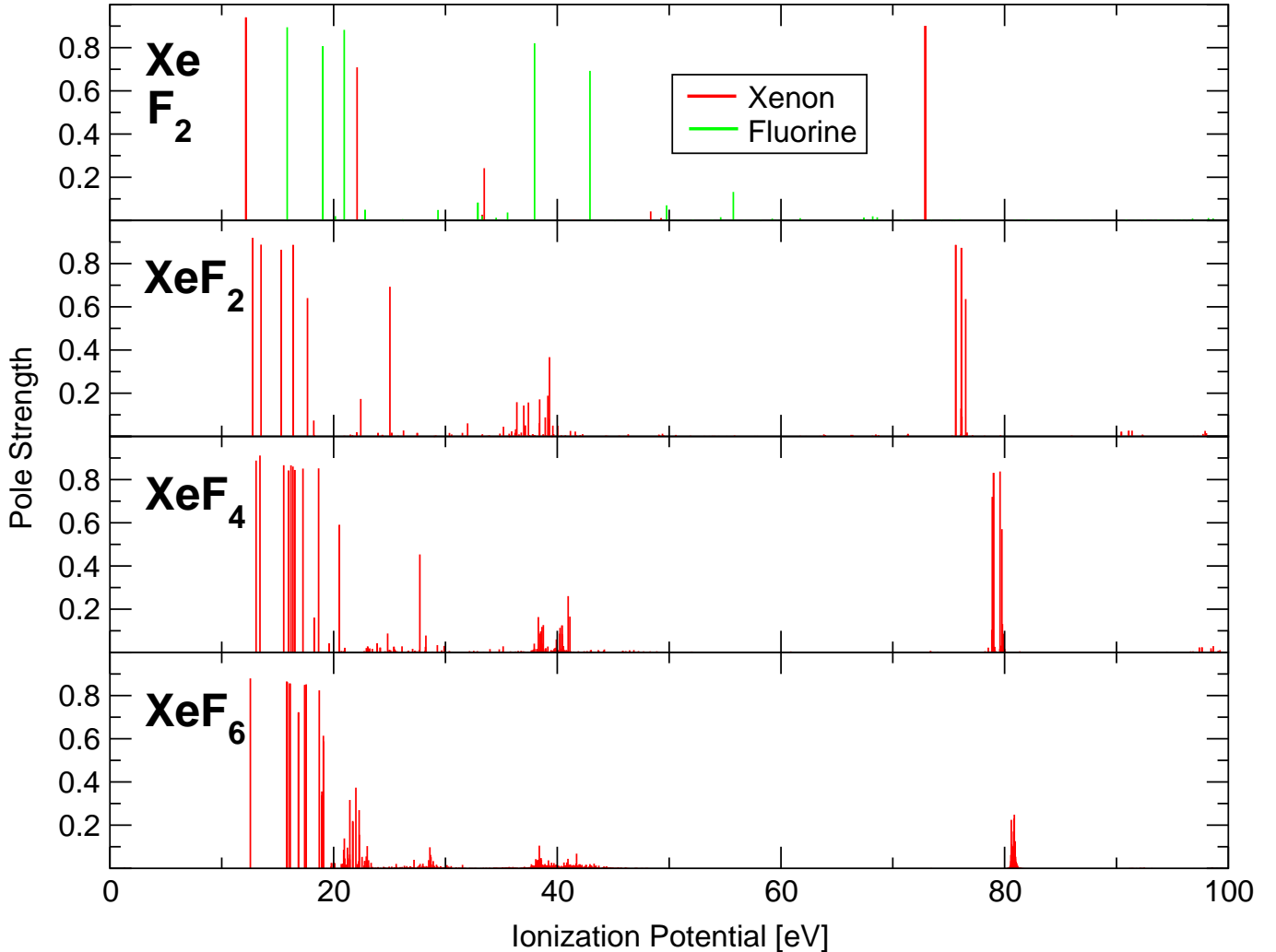


FIG. 2: (Color) Single ionization spectra of Xe, F₂, XeF₂, XeF₄, and XeF₆ calculated with the one-particle ADC(3) program (see the text). The assignment of lines to atomic orbitals of xenon or fluorine origin is not done for the XeF_n molecules.

breakdown of the molecular orbital picture of ionization is caused by compact two-hole-one-particle configurations that are close in energy to a one-hole state³⁹. The strong Coulomb coupling of these configurations to one-hole states leads to a broad shape of lines, which has been discovered in the inner-valence region of many molecules³⁹.

Due to the many-body description of a molecule by the ADC scheme, decay processes of electronic states of the ion that lie above the double ionization threshold also become describable⁴⁰. In particular, the final state of the electronic decay of an ionized molecule can be approximated in terms of two-hole-one-particle configurations describing the emitted electron (the particle) and the residual dication (the two holes)⁴¹. The shape of each decaying state can be identified as a thin bundle of lines, which mimic a discretized Lorentzian curve⁴⁰.

In order to unambiguously identify a decaying state,

the breakdown of the molecular orbital picture of ionization has to be separated clearly from the decaying states in a small energy range where each decaying state is represented by a discretized Lorentzian curve. Furthermore, there can be a mixing of both phenomena for a certain state, but it is hard to identify a decay curve for one-hole states that suffer from the breakdown phenomenon.

The inner-valence region of the xenon fluorides comprises the Xe 5s and F 2s states. The F 2s states are subject to the breakdown phenomenon and can also decay by emitting an electron^{28,42}. The Xe 5s one-hole state suffers solely from breakdown. No decay is possible because its ionization potential is below the double ionization threshold^{28,42}. Many two-hole-one-particle configurations can couple to the Xe 5s one-hole state (see Fig. 2). As the Xe 5s line is close to the double ionization threshold^{28,42}, many two-hole-one-particle configurations are close in energy to this state: The excited states are gen-

erally very dense in this energetic region.

The spectra exhibit a considerable increase of breakdown of the molecular orbital picture for the inner valence with an increasing number of fluorine atoms. Obviously, the number of suitable configurations rises due to the addition of fluorine atoms. Since xenon fluorides are very symmetric, these fluorine atoms are all equivalent (except for XeF_6 in C_{3v} symmetry), and the number of equivalent two-hole-one-particle configurations with one hole on the xenon atom and one hole on a fluorine atom doubles between XeF_2 and XeF_4 . In XeF_6 there are even more such configurations than there are in XeF_4 , but they are no longer equivalent due to the C_{3v} symmetry of the XeF_6 ground state.

Another contribution to the increase of one-hole states involved in the breakdown phenomenon can be attributed to the decrease in symmetry: spherical symmetry (Xe), $D_{\infty h}$ (XeF_2), D_{4h} (XeF_4), C_{3v} (XeF_6). This decrease in symmetry leads to an increase in excited electronic configurations that can couple to the respective one-hole states.

The one-particle picture provides a rather good description for the $\text{Xe}4d$ lines. Two-hole-one-particle configurations close to the energy of the core one-hole configurations are spatially diffuse and thus couple only weakly to the core one-hole configurations. Therefore, in the core regime, the mixing of two-hole-one-particle configurations with one-hole configurations is relatively weak. The splittings of the $\text{Xe}4d$ lines in the xenon fluorides are of comparable size to those in Fig. 1, and the individual lines can be identified easily in all molecules but XeF_6 .

Since in all xenon fluorides the $\text{Xe}4d$ lines are above the double ionization threshold^{28,42}, $\text{Xe}4d$ -ionized xenon fluorides can undergo Auger decay. The $\text{Xe}4d$ lines in Fig. 2 show signs of decay by exhibiting features of discretized Lorentzian curves. The shape of the approximate Lorentzian curve representing a decaying state in the spectra depends highly on the number of two-hole-one-particle configurations in the energy range of the decay electron.

The decay electrons that result from the decay of a $\text{Xe}4d$ vacancy are highly energetic (up to ≈ 60 eV). Hence, a satisfactory description in terms of Gaussian basis sets is not feasible. For this reason, the $\text{Xe}4d$ ionization potentials in Fig. 2 correspond in our description essentially to one-hole states (a pole strength close to unity). Nevertheless, the number of states which originate from two-hole-one-particle configurations around the $\text{Xe}4d$ ionization potentials grows substantially with the number of fluorine atoms. In XeF_6 one observes very densely lying states around 83 eV with a high contribution of two-hole-one-particle configurations. The extreme change in the importance of two-hole-one-particle configurations in XeF_6 compared to XeF_4 , XeF_2 was investigated by us.

The six fluorine atoms in XeF_6 form a distorted octahedron around the xenon atom. The basis set of the fluorine atoms may therefore help improve the descrip-

tion of the decay electron from $\text{Xe}4d$ -ionized XeF_6 considerably. To test this assumption, we calculated the ionization spectrum of XeF_2 with the DZVP (DFT orbital) basis set augmented by a few diffuse functions. The resulting spectrum did not change much compared to that of Fig. 2.

To test the effect of the basis functions on the fluorine atoms, we performed another calculation of the ionization spectrum of XeF_2 with fluorine basis functions attached to ghost centers arranged such as to yield an octahedron of fluorine basis functions surrounding the central xenon atom. The extra basis functions had a minor effect on the spectrum and did not account for the drastic effect observed in Fig. 2 for XeF_6 .

These investigations convinced us of the suitability of the DZVP (DFT orbital) basis set for our concerns but did not clarify the reasons for the drastic change in Fig. 2. To this end, we calculated the ionization spectrum of XeF_6 in O_h geometry. The resulting $\text{Xe}4d$ lines had a shape similar to that of the $\text{Xe}4d$ lines in XeF_4 , revealing the great importance of the decreased symmetry for the description of XeF_6 in our computations. The reduction in symmetry from O_h to C_{3v} enables a vastly enlarged amount of two-hole-one-particle configurations to couple to the $\text{Xe}4d$ one-hole configurations. To some extent, this is similar to an increased basis set, as a multitude of configurations are provided additionally for the description of the ionized states. For sure, this improves the description of those decay electrons with low kinetic energy.

The charge transfer from the xenon atom to the fluorine atoms in the ground state, discussed in Sec. III A, leaves a positively charged central xenon atom. Therefore, it is not surprising that XeF_4 and XeF_6 possess positive electron affinities, i.e. $(\text{XeF}_4)^-$ and $(\text{XeF}_6)^-$ are electronically stable anions. We have computed the respective electron affinities by ADC(3). The value obtained for XeF_4 (a doubly degenerate state) is 0.66 eV; the electron affinities of XeF_6 lie at 1.30 eV, 1.31 eV, and 1.81 eV, respectively. The figures are presumably not very accurate because the DZVP (DFT orbital) basis set is not particularly well suited for describing the diffuse states of anions. In XeF_6 , the fluorine atoms form a cage of negative charge, of nearly octahedral symmetry, surrounding the central, positively charged xenon atom. The resulting potential well is similar to the model potential well discussed in Refs. 28,43. In these references, both bound states as well as scattering resonances in the model potential well were investigated.

The $\text{Xe}4d$ and $\text{F}2s$ lines in Fig. 2 are shifted to higher ionization potentials with increasing number of fluorine atoms (see Sec. III A). This general trend, seen in the mean-field approximation of Fig. 1, can still be identified if electron correlation is taken into account. Nevertheless, the difference between the shifts of the $\text{Xe}4d$ lines of XeF_2 and XeF_4 is larger than that between the $\text{Xe}4d$ lines of XeF_4 and XeF_6 . Electron correlation reduces the effect caused by charge depletion on

Cmpd.	Line	IP_{exp}	IP_{ADC}	IP_{rel}	Γ_{exp}
Xe	1	69.525 (10)	72.90	69.82	0.207 (4)
	2	67.541 (9)			0.202 (4)
XeF_2	1	72.568 (6)	76.52	73.44	0.248 (8)
	2	72.248 (6)	76.14	73.06	0.223 (10)
	3	70.601 (13)	75.63	72.55	0.264 (26)
	4	70.421 (9)			0.256 (27)
	5	70.179 (6)			0.214 (19)
XeF_4	1	75.098 (6)	79.76	76.68	0.319 (8)
	2	74.729 (7)	79.60	76.52	0.255 (8)
	3	73.140 (10)	79.01	75.93	0.392 (10)
	4	72.816 (10)	78.89	75.81	0.210 (27)
	5	72.661 (5)			0.225 (26)
XeF_6	1	77.462 (13)	80.86	77.78	0.32 (4)
	2	77.321 (11)	80.59	77.51	0.25 (3)
	3	75.53			0.33
	4	75.38			0.25
	5	75.25			0.25

TABLE IV: Peak positions and widths of the $\text{Xe}4d$ lines in Xe , XeF_2 , XeF_4 , and XeF_6 . *Labels* – Cmpd.: compound; IP_{exp} : experimental peak position; IP_{ADC} : calculated peak position; IP_{rel} : calculated peak position with relativistic correction; Γ_{exp} : experimental peak width. IP_{exp} and Γ_{exp} are photoelectron-experimental data, reproduced from Table 1 in Ref. 6. For XeF_6 , the data with an experimental resolution of 0.11 eV are taken. The values in brackets are the standard deviations of the peak positions and peak widths⁶. IP_{ADC} and IP_{rel} are sorted descending in energy for each compound. The value of IP_{exp} does not necessarily correspond to the values of IP_{ADC} and IP_{rel} in the same row as spin-orbit splitting is neglected to obtain the latter ones. All data are given in electronvolt.

the xenon atom.

The non-relativistic IP_{ADC} are listed in Table IV together with the IP_{rel} obtained by applying to IP_{ADC} the relativistic correction $-\Delta\epsilon$ of Sec. II C. The number of distinct $\text{Xe}4d$ lines is smaller in the non-relativistic spectra due to a higher degeneracy caused by neglecting the spin-orbit coupling. The $\text{Xe}4d$ lines of XeF_6 cannot be identified clearly in Fig. 2. One expects from Sec. III A two lines for a ground-state geometry of O_h symmetry and three lines for a ground-state geometry of C_{3v} symmetry. The two ionization potentials, in the energy range of the $\text{Xe}4d$ lines of XeF_6 (80–83 eV), with maximum pole strength are listed in Table IV.

The $\text{Xe}4d$ IP_{rel} differ from the experimentally obtained data in Table IV by only 1.5–2.5 eV ($\approx 3\%$), which is a good agreement in view of the complexity of the problem and the necessity to describe the decay simultaneously. The reason for the deviation is twofold. First, the spin-orbit splitting is neglected, which amounts to 2.111 eV for the $\text{Xe}4d$ lines of the xenon atom, according to Sec. II C. Second, since the calculations are based on the

ADC(3) approximation, the three-hole–two-particle configurations are neglected (ADC(4) calculations are currently beyond reach). The inclusion of these additional configurations would shift the ionization potentials of the $\text{Xe}4d$ lines further to lower energy, due to an improved description of core-hole relaxation²⁴.

Let us now turn our attention to the last column in Table IV: the experimental widths of the $\text{Xe}4d$ photo-electron peaks⁶. It is evident that, on average, the widths increase from Xe to XeF_6 . According to Cutler *et al.*⁶, this effect probably cannot be explained in terms of vibrational broadening. If the data reflect more or less pure Auger widths, then the experimental findings are in contradiction to expectations based on the one-center model⁴⁴. The electronegative fluorine ligands withdraw charge from xenon (see Table II). Correspondingly, fewer valence electrons are available for a local, atomic mechanism of $\text{Xe}4d$ Auger decay. Hartmann’s semiempirical multi-center model⁴⁵, on the other hand, predicts a larger $\text{C}1s$ Auger width for CF_4 than for CH_4 , which, though seemingly in line with the trend in XeF_n , is inconsistent with experiment⁴⁶.

In our work on neon clusters, we demonstrated not only that a $\text{Ne}2s$ hole *in a cluster* can decay by electron emission⁴⁷—a fact confirmed by a recent experiment⁴⁸—but also that the decay lifetime depends sensitively on the number of nearest neighbors surrounding the atom carrying the inner-valence hole⁴¹. The $\text{Ne}2s$ lifetime drops in a monotonic manner from about 80 fs in Ne_2^+ to less than 5 fs in Ne_{13}^+ . The mechanism responsible for this dramatic effect is referred to as *Interatomic Coulombic Decay*. In heteroclusters, additional electronic mechanisms play a role⁴⁹. We will demonstrate in an upcoming paper⁴² how the decay mechanisms discovered in clusters elucidate the counterintuitive behavior of the $\text{Xe}4d$ Auger widths in XeF_n .

Here, we would like to emphasize that traces of a purely electronic origin can already be found in our ADC(3) spectra, Fig. 2. As the number of fluorine ligands grows, there are more and more two-hole–one-particle configurations that can couple to the $\text{Xe}4d$ holes. In other words, the number of dicationic decay channels grows, and therefore we observe in Fig. 2 an increasing loss of main-line intensity and the emergence of dense line bundles. This is the signature in our finite-basis-set calculations of enhanced electronic decay⁴⁰, as pointed out previously.

IV. CONCLUSION

The xenon fluorides are very special systems. Not only are they rather peculiar chemical compounds, they are also particularly well suited to investigating the systematic evolution of many-body effects.

While outer-valence ionization is mostly compatible with the mean-field approach, the situation is strikingly different in the inner-valence region. At the Hartree-Fock level, the chemical environment leads to mere shifts of the

Xe 5s and F 2s lines. The ADC(3) calculation, however, reveals that electron correlation can induce additional, pronounced environmental effects. Xe 5s ionization in XeF₂ can be relatively well understood in terms of a one-particle picture. In XeF₄, this picture begins to crumble, and in XeF₆, there is not a single cationic eigenstate that overlaps well with the Xe 5s one-hole configuration.

The F 2s states are even more interesting, since they are higher in energy than the double ionization threshold. In the xenon fluorides, electron correlation enforces the excitation of a large, system-dependent number of F 2s-derived electronic states. All of these states are resonances decaying by electron emission. Neither the decay mechanism nor the decay timescale are known. Resolving these issues may have important consequences for other molecules. This poses an exciting challenge to both theory and experiment.

This is the first paper dealing with the inner-valence physics of XeF_n at a correlated level. We are not aware of any experimental spectra in this energy region. The quality of our calculations can be assessed, however, by reference to our ADC(3) results for the Xe 4d core lines. Upon correction for scalar relativistic effects, our numerical data agree with experiment within a few percent. The

remaining difference can be attributed to an incomplete description of core-hole relaxation and to our neglect of spin-orbit coupling. The ADC(3) scheme is capable of reproducing the experimentally observed line shifts as well as the counterintuitive Auger broadening. A detailed analysis of the latter phenomenon will be presented elsewhere.

Acknowledgments

We are highly indebted to T. Darrah Thomas for drawing our attention to the xenon fluorides. He pointed out Ref. 6 and supported it further with valuable private communications. Markus Pernpointner helped estimate the impact of the relativistic effects in the xenon atom. This work would not have been possible without the ADC programs and support by Francesco Tarantelli. Imke B. Müller, Sven Feuerbacher, Jörg Breidbach, and Thomas Sommerfeld accompanied our work with helpful comments and fruitful discussions. R. S. and L. S. C. gratefully acknowledge financial support by the Deutsche Forschungsgemeinschaft (DFG).

* Corresponding author: Christian.Buth@ePost.de; Present address: Max-Planck-Institut für Physik komplexer Systeme, Nöthnitzer Straße 38, 01187 Dresden, Germany

† Present address: JILA, University of Colorado, Boulder, CO 80309-0440, USA

¹ N. Wiberg, A. F. Holleman, and E. Wiberg, *Inorganic Chemistry* (Academic Press, New York, 2001), ISBN 0-123-52651-5.

² F. J. Comes, R. Haensel, U. Nielsen, and W. H. E. Schwarz, *J. Chem. Phys.* **58**, 516 (1973).

³ U. Nielsen, R. Haensel, and W. H. E. Schwarz, *J. Chem. Phys.* **61**, 3581 (1974).

⁴ U. Nielsen and W. H. E. Schwarz, *Chem. Phys.* **13**, 195 (1976).

⁵ T. X. Carroll, R. W. Shaw Jr., T. D. Thomas, C. Kindle, and N. Bartlett, *J. Am. Chem. Soc.* **96**, 1989 (1974).

⁶ J. N. Cutler, G. M. Bancroft, J. D. Bozek, K. H. Tan, and G. J. Schrobilgen, *J. Am. Chem. Soc.* **113**, 9125 (1991).

⁷ H. Basch, J. W. Moskowitz, C. Hollister, and D. Hankin, *J. Chem. Phys.* **55**, 1922 (1971).

⁸ L. Scheire, P. Phariseau, R. Nuyts, A. E. Foti, and V. H. Smith Jr., *Physica A* **101**, 22 (1980).

⁹ G. L. Gutsev and A. E. Smoijar, *Chem. Phys.* **56**, 189 (1981).

¹⁰ M. Kaupp, C. van Wüllen, R. Franke, F. Schmitz, and W. Kutzelnigg, *J. Am. Chem. Soc.* **118**, 11939 (1996).

¹¹ J. Styszyński, X. Cao, G. L. Malli, and L. Visscher, *J. Comput. Chem.* **18**, 601 (1997).

¹² M.-S. Liao and Q.-E. Zhang, *J. Phys. Chem. A* **102**, 10647 (1998).

¹³ A. L. Fetter and J. D. Walecka, *Quantum Theory of Many-Particle Systems*, International Series in Pure and Applied

Physics, edited by Leonard I. Schiff (McGraw-Hill, New York, 1971).

¹⁴ R. D. Mattuck, *A Guide to Feynman Diagrams in the Many-Body Problem* (McGraw-Hill, New York, 1976), 2nd ed., ISBN 0-07-040954-4.

¹⁵ E. K. U. Gross, E. Runge, and O. Heinonen, *Many-Particle Theory* (Adam Hilger, Bristol, 1991), ISBN 0-7503-0155-4.

¹⁶ A. Szabo and N. S. Ostlund, *Modern Quantum Chemistry: Introduction to Advanced Electronic Structure Theory* (Macmillan, New York, 1982), ISBN 0-02-949710-8.

¹⁷ L. S. Cederbaum and W. Domcke (Wiley, New York, 1977), vol. 36 of *Adv. Chem. Phys.*, pp. 205–344.

¹⁸ L. S. Cederbaum, in *Encyclopedia of Computational Chemistry*, edited by P. v. R. Schleyer (Wiley, New York, 1998), ISBN 0-471-96588-X.

¹⁹ J. Schirmer, *Phys. Rev. A* **26**, 2395 (1982).

²⁰ J. Schirmer, L. S. Cederbaum, and O. Walter, *Phys. Rev. A* **28**, 1237 (1983).

²¹ J. Schirmer and G. Angonoa, *J. Chem. Phys.* **91**, 1754 (1989).

²² H.-G. Weikert, H.-D. Meyer, L. S. Cederbaum, and F. Tarantelli, *J. Chem. Phys.* **104**, 7122 (1996).

²³ L. S. Cederbaum, W. Domcke, and J. Schirmer, *Phys. Rev. A* **22**, 206 (1980).

²⁴ G. Angonoa, O. Walter, and J. Schirmer, *J. Chem. Phys.* **87**, 6789 (1987).

²⁵ J. Schirmer and A. Thiel, *J. Chem. Phys.* **115**, 10621 (2001).

²⁶ F. Tarantelli, private communication.

²⁷ GAMESS-UK is a package of ab initio programs written by M. F. Guest, J. H. van Lenthe, J. Kendrick, K. Schoffel, and P. Sherwood, with contributions from R. D. Amos, R. J. Buenker, H. J. J. van Dam, M. Dupuis, N. C. Handy,

I. H. Hillier, P. J. Knowles, V. Bonacic-Koutecky, W. von Niessen, R. J. Harrison, A. P. Rendell, V. R. Saunders, A. J. Stone, D. J. Tozer, and A. H. de Vries. The package is derived from the original GAMESS code due to M. Dupuis, D. Spangler and J. Wendoloski, NRCC Software Catalog, Vol. 1, Program No. QG01 (GAMESS), 1980.

²⁸ C. Buth, Diplomarbeit, Ruprecht-Karls Universität Heidelberg, Theoretische Chemie, Physikalisch-Chemisches Institut, Im Neuenheimer Feld 229, 69120 Heidelberg, Germany (2002), www.ub.uni-heidelberg.de/archiv/3004.

²⁹ N. Godbout, D. R. Salahub, J. Andzelm, and E. Wimmer, Can. J. Chem. **70**, 560 (1992).

³⁰ Basis sets were obtained from the *Extensible Computational Chemistry Environment Basis Set Database*, Version 5/22/02, as developed and distributed by the Molecular Science Computing Facility, Environmental and Molecular Sciences Laboratory which is part of the Pacific Northwest Laboratory, P.O. Box 9999, Richland, Washington 99352, USA, and funded by the U.S. Department of Energy. The Pacific Northwest Laboratory is a multi-program laboratory operated by Battelle Memorial Institute for the U.S. Department of Energy under contract DE-AC06-76RLO 1830. Contact David Feller or Karen Schuchardt for further information.

³¹ K. Balasubramanian, *Relativistic Effects in Chemistry: Theory and Techniques* (John Wiley & Sons, New York, 1997), ISBN 0-471-30400-X.

³² P. Pyykkö, Chem. Rev. **88**, 563 (1988).

³³ C. Froese-Fischer, Comp. Phys. Commun. **14**, 145 (1978).

³⁴ K. G. Dyall, I. P. Grant, T. Johnson, C., F. A. Parpia, and E. P. Plummer, Comp. Phys. Commun. **55**, 425 (1989).

³⁵ F. A. Parpia, C. Froese-Fischer, and I. P. Grant, Comp. Phys. Commun. **94**, 249 (1996).

³⁶ T. Koopmans, Physica **1**, 104 (1933).

³⁷ R. S. Mulliken, J. Chem. Phys. **23**, 1833 (1955).

³⁸ J. J. Sakurai, *Modern Quantum Mechanics* (Addison-Wesley, Reading (Massachusetts), 1994), 2nd ed., ISBN 0-201-53929-2.

³⁹ L. S. Cederbaum, W. Domcke, J. Schirmer, and W. von Niessen (Wiley, 1986), vol. 65 of *Adv. Chem. Phys.*, pp. 115–159.

⁴⁰ J. Zobeley, L. S. Cederbaum, and F. Tarantelli, J. Chem. Phys. **108**, 9737 (1998).

⁴¹ R. Santra, J. Zobeley, and L. S. Cederbaum, Phys. Rev. B **64**, 245104 (2001).

⁴² C. Buth, R. Santra, and L. S. Cederbaum (2003), manuscript in preparation.

⁴³ R. Santra and L. S. Cederbaum, Phys. Rep. **368**, 1 (2002).

⁴⁴ M. Coville and T. D. Thomas, Phys. Rev. A **43**, 6053 (1991).

⁴⁵ E. Hartmann, J. Phys. B **21**, 1173 (1988).

⁴⁶ T. X. Carroll, K. J. Børve, L. J. Sæthre, J. D. Bozek, E. Kukk, J. A. Hahne, and T. D. Thomas, J. Chem. Phys. **116**, 10221 (2002).

⁴⁷ R. Santra, J. Zobeley, L. S. Cederbaum, and N. Moiseyev, Phys. Rev. Lett. **85**, 4490 (2000).

⁴⁸ S. Marburger, O. Kugeler, U. Hergenhahn, and T. Möller, Phys. Rev. Lett. **90**, 203401 (2003).

⁴⁹ J. Zobeley, R. Santra, and L. S. Cederbaum, J. Chem. Phys. **115**, 5076 (2001).